Towards accurate orbital-free simulations: A generalized gradient approximation for the noninteracting free energy density functional

K. Luo,[1,*] V. V. Karasiev,[2,†] and S. B. Trickey[3,‡]

[1]*Geophysical Laboratory, Carnegie Institution, 5251 Broad Branch Road NW, Washington D.C. 20015, USA*

[2]*Laboratory for Laser Energetics, University of Rochester, Rochester, New York 14623, USA*

[3]*Quantum Theory Project, Department of Physics and Department of Chemistry, University of Florida, Gainesville, Florida 32611, USA*

(Received 3 December 2019; accepted 29 January 2020; published 13 February 2020)

For orbital-free *ab initio* molecular dynamics, especially on systems in extreme thermodynamic conditions, we provide an innovative pseudopotential-adapted generalized gradient approximation (GGA) functional for the noninteracting free energy. This is achieved by systematic finite-temperature extension of our recent LKT ground-state noninteracting kinetic energy GGA functional [Phys. Rev. B **98**, 041111(R) (2018)]. We test the performance of the functional first via static lattice calculations on crystalline aluminum and silicon. Then we compare deuterium equation of state results against both path-integral Monte Carlo and conventional (orbital-dependent) Kohn-Sham results. The functional, denoted LKTF, outperforms the previous best semilocal free energy functional VT84F [Phys. Rev. B **88**, 161108(R) (2013)], and provides modestly faster simulations. We also discuss subtleties of identification of kinetic and entropic contributions to noninteracting free energy functionals obtained by extension from ground-state orbital-free kinetic energy functionals.

DOI: 10.1103/PhysRevB.101.075116

I. CONTEXT AND MOTIVATION

Warm dense matter (WDM) has been a research topic of substantial recent interest because of its importance in high energy density sciences and its inherently quantum mechanical nature [1]. WDM has been a challenge both experimentally and theoretically. Despite progress, it remains so. Though advances in experimental facilities and techniques are making parts of the relevant state space accessible, the value and urgency of reliable, computationally affordable theoretical methods still is undeniable. However, conventional methods are unaffordable for application over the entirety of the typical temperature range of interest. For example, path-integral Monte Carlo (PIMC) takes advantage of the Trotter expansion at very high temperatures but becomes intractable lower into the WDM regime. Conversely, stochastic density functional theory (DFT) remains computationally expensive at low temperature [2,3].

For ordinary condensed matter conditions, ground-state DFT [4] in its conventional Kohn-Sham (KS) realization [5] has achieved enormous success. That is thanks to the elegant balance between computational cost and accuracy provided by KS DFT. By extension, the *de facto* standard methodology for WDM, e.g., for prediction of equations of state, is *ab initio* molecular dynamics (AIMD) with forces from Mermin free energy DFT [6].

For general state conditions, however, the conventional KS implementation of FT-DFT, with its explicit orbital dependence in the form of solution of the KS equations, scales computationally no better than $N_{\rm occ}^3$, with $N_{\rm occ}$ the number of occupied KS orbitals. For gapped systems, locality or sparsity can be exploited to achieve linear scaling [7] but this approach lacks the generality of applicable state conditions essential for WDM. As the electron temperature (and/or system size) grows, at some point KS-AIMD calculations become impractical (unaffordable) because of the enormous number of non-negligibly occupied KS states. Orbital-free molecular dynamics (OFMD) is an attractive alternative because its computational cost scales linearly with system size irrespective of the particular system state.

With recent advances in approximate noninteracting kinetic density functionals $T_{\rm s}$, ground-state OFMD is beginning to be a viable alternative to low-T KS-AIMD. Both semilocal and nonlocal functionals have achieved mixed success in treating condensed phases and their ingredient atoms, molecules, and clusters and solids. Such functionals are either constraint based and nonempirical [8–18] or semiempirical [19,20]. With any significant ground-state advance, an obvious, important associated step is generalization to a noninteracting free energy functional $\mathcal{F}_{\rm s}$. In this work, we make that step based upon a recently proposed ground-state $T_{\rm s}$ functional, LKT [10]. It has the novel property of being adapted specifically to working with pseudodensities, such as almost always are used in AIMD calculations. Thus LKT satisfies known constraints on $\mathcal{F}_{\rm s}$ for pseudodensities, not physical densities. Hence LKT is nonuniversal by construction to achieve good performance from a semilocal functional. But it is *not empirical*.

The next section summarizes free energy DFT to establish notation, conventions, and correspondence with ground-state KS-DFT. It then summarizes the T-dependent dimensionless

*kluo@carnegiescience.edu

†vkarasev@lle.rochester.edu

‡trickey@qtp.ufl.edu

gradient variables developed in Ref. [9] and uses them to generalize the LKT T_s to $\mathcal{F}_s$. Section III summarizes matters of computational technique, after which Sec. IV presents calculated results and comparisons. We conclude with discussion and summary in Sec. V.

II. FREE ENERGY DENSITY FUNCTIONALS

In the grand canonical ensemble, the electronic grand potential Ω for a system of average electron number $\langle N\rangle$ under external potential v is minimized by the equilibrium electronic number density $n_{\rm eq}$, that is, there is a one-to-one mapping between v and $n_{\rm eq}$ (see Ref. [6] for details). The electronic grand potential can be written as a density functional

$$\Omega[n,T] = \mathcal{F}[n,T] + \int d\mathbf{r}\,[v(\mathbf{r})-\mu]n(\mathbf{r}), \tag{1}$$

where μ and T are the chemical potential and electronic system temperature. The universal free energy functional $\mathcal{F}[n,T]$ can be constructed formally by constrained search. As in the ground-state KS scheme, the free energy functional is decomposed into three pieces,

$$\mathcal{F}[n,T] = \mathcal{F}_s[n,T] + \mathcal{F}_H[n] + \mathcal{F}_{xc}[n,T], \tag{2}$$

where $\mathcal{F}_s$, $\mathcal{F}_H$, and $\mathcal{F}_{xc}$ are the noninteracting free energy, the classical Coulomb free energy (or Hartree energy), and the exchange-correlation (XC) free energy, respectively. $\mathcal{F}_H$ has a simple, explicit density dependence, hence needs no attention.

In the conventional use of the KS decomposition, the noninteracting free energy $\mathcal{F}_s = \mathcal{T}_s - T\mathcal{S}_s$, is treated exactly, with the orbital-dependent, noninteracting KE and entropy given by

$$\mathcal{T}_s[n,T] = -\frac{1}{2}\sum_{j=1}^{N_{\rm occ}}\int d\mathbf{r}\, f_j\varphi_j^*(\mathbf{r})\nabla^2\varphi_j(\mathbf{r}) \tag{3}$$

and

$$\mathcal{S}_s[n,T] = -k_B\sum_{j=1}^{N_{\rm occ}}[f_j\ln f_j + (1-f_j)\ln(1-f_j)]. \tag{4}$$

Here φ_j are thermally occupied KS orbitals with $j = 1,\ldots,N_{\rm occ}$. The Fermi-Dirac distribution function is $f_j = 1/(1+e^{\beta(\varepsilon_j-\mu)})$ where ε_j is the jth eigenvalue of the KS equation and $\beta = 1/(k_BT)$ is the inverse temperature with Boltzmann constant k_B. In computational practice, the chemical potential μ is determined via $\sum_{j=1}^{N_{\rm occ}} f_j = N$, the number of electrons.

In this context, the only approximation needed is for the XC free energy $\mathcal{F}_{xc}[n,T]$. There has been recent progress on both local density approximations (based on the homogeneous electron gas, HEG) in Refs. [21–23] and on a generalized gradient approximation [24] for $\mathcal{F}_{xc}[n,T]$.

Solution of the conventional KS eigenvalue problem requires diagonalization or equivalent. That is the source of the computational cost scaling no better than $N_{\rm occ}^3$ already noted. Such scaling poses a major obstacle to routine WDM simulation, as already remarked. Orbital-free DFT (OFDFT) offers the potential to remove this barrier.

A. Generalized gradient approximations

Two approximate functionals are required in free energy OFDFT, $\mathcal{F}_s$ and $\mathcal{F}_{xc}$. Our focus is on the first.

The most widely used, though far from optimal $\mathcal{F}_s$ approximation in free energy OFDFT, is the Thomas-Fermi (TF) functional [25]. By making a local density approximation based on the HEG as paradigm, evaluation of Eq. (1), $\Omega^{\rm HEG}$, leads to the TF approximate free energy

$$\mathcal{F}_s^{\rm TF}[n,T] = \int d\mathbf{r}\, f_s^{\rm TF}(n,T), \tag{5}$$

and associated free energy density

$$f_s^{\rm TF}(n,T) = \frac{\sqrt{2}}{\pi^2\beta^{5/2}}\left[-\frac{2}{3}I_{3/2}(\beta\mu) + \beta\mu I_{1/2}(\beta\mu)\right]. \tag{6}$$

(Note that free energy densities are unique only up to a gauge transformation; here and throughout we use conventional forms.) The Fermi-Dirac integrals [26,27] are

$$I_\alpha(\eta) \equiv \int_0^\infty \frac{x^\alpha}{1+e^{x-\eta}}\,dx. \tag{7}$$

The chemical potential μ can be determined from

$$n = -\frac{1}{V}\left.\frac{\partial\Omega^{\rm HEG}}{\partial\mu}\right|_{T,V} = \frac{\sqrt{2}}{\pi^2\beta^{3/2}}I_{1/2}(\beta\mu). \tag{8}$$

In terms of the reduced temperature

$$t = T/T_F = \frac{2}{\beta[3\pi^2 n]^{2/3}}, \tag{9}$$

$I_{1/2}(\beta\mu) = n\pi^2\beta^{3/2}/\sqrt{2} = 2t^{-3/2}/3$ and Eq. (6) becomes

$$f_s^{\rm TF}(n,T) = \tau_0^{\rm TF}(n)\kappa(t), \tag{10}$$

with

$$\tau_0^{\rm TF}(n) = \frac{3}{10}(3\pi^2)^{2/3}n^{5/3} \tag{11}$$

and

$$\kappa(t) = \frac{5}{2}t^{5/2}\left[-\frac{2}{3}I_{3/2}(\beta\mu) + \beta\mu I_{1/2}(\beta\mu)\right]. \tag{12}$$

Beyond the HEG, the second-order gradient approximation (SGA) for the noninteracting free-energy density is

$$f_s^{\rm SGA}(n,\nabla n,T) = f_s^{\rm TF}(n,T) + 8h(t)\frac{|\nabla n|^2}{8n}, \tag{13}$$

with

$$h(t) = -\frac{1}{24}\frac{I_{1/2}(\beta\mu)I_{-3/2}(\beta\mu)}{I_{-1/2}^2(\beta\mu)}. \tag{14}$$

It is convenient to use $\tilde{h} = 72h$ because $\lim_{t\to 0}\tilde{h}(t) = 1$.

The well-documented limitations of the SGA motivate generalized gradient approximations (GGAs). Some time ago, a systematic means of promoting a ground-state GGA noninteracting functional to become a noninteracting free energy GGA was put forth [9]. Ground-state functionals are expressed as a function of the dimensionless reduced density gradient

$$s(n,\nabla n) := \frac{|\nabla n|}{(2k_F)n} = \frac{1}{2(3\pi^2)^{1/3}}\frac{|\nabla n|}{n^{4/3}}, \tag{15}$$

By examination of the finite-T gradient expansion, Ref. [9] identified the proper finite-T reduced density gradients for the kinetic and entropic contributions, to wit,

$$s_\tau(n,\nabla n,T)=s(n,\nabla n)\sqrt{\frac{\tilde{h}(t)-t\tilde{h}'(t)}{\xi(t)}}, \tag{16}$$

$$s_\sigma(n,\nabla n,T)=s(n,\nabla n)\sqrt{\frac{t\tilde{h}'(t)}{\zeta(t)}}. \tag{17}$$

Here the t-dependent functions are

$$\xi(t)=\kappa(t)-t\kappa'(t), \tag{18}$$

$$\zeta(t)=-t\kappa'(t), \tag{19}$$

and primes denote differentiation with respect to the indicated variable. The finite-temperature GGA free energy functional then has a kinetic and entropic term,

$$\mathcal{F}_{\rm s}^{\rm GGA}[n,T]=\int d\mathbf{r}\ \tau_0^{\rm TF}[\xi(t)F_\tau(s_\tau)-\zeta(t)F_\sigma(s_\sigma)], \tag{20}$$

with distinct enhancement factors F_τ and F_σ.

Evidently, the zero-T GGA enhancement factor is only for the kinetic energy, that is $F_\tau(s_\tau)\to F_t(s)$. In addition, therefore, to the replacement $s\to s_\tau$, the entropic enhancement factor F_σ must be constructed. A thermodynamic Maxwell relation relates the two exactly but the resulting differential equation is not trivial to solve [9]. An identity for the SGA [9]

$$F_\sigma(s_\sigma)=2-F_\tau(s_\sigma) \tag{21}$$

is a useful approximation for GGA construction. To date it has proven reasonably successful. For instance, VT84F, an earlier GGA free energy functional, used (21) to yield reasonably good performance in the WDM regime [28]. Detailed numerical assessment of Eq. (21) in the present case is given in the Supplemental Material [29].

For clarity of analysis, we include the ground-state approximate functionals TFλvW, with $\lambda=1/5$ or $1/9$. Their enhancement factor is

$$F_{\rm t}^{\rm TF\lambda vW}(s)=1+\lambda\frac{5}{3}s^2. \tag{22}$$

Here "vW" denotes the von Weizsäcker KE functional. We note that such TF plus scaled vW functionals with $\lambda<1$ violate the positivity requirements on the Pauli potential v_θ that is the functional derivative of the Pauli KE T_θ in the rigorous decomposition [8]

$$T_{\rm s}=T_{\rm vW}+T_\theta,\quad T_\theta\geqslant 0. \tag{23}$$

Nonetheless, there is a literature of using TF$\frac{1}{5}$vW for the ground state, hence it is a useful context to assess its performance when extended to finite T. Note also that TF$\frac{1}{9}$vW is the Perrot functional [30].

B. Adaptation to pseudodensities

The aforementioned exact positivity conditions for the ground-state KE functional are $T_\theta\geqslant 0$ and $\delta T_\theta/\delta n\geqslant 0\,\forall\mathbf{r}$. These are powerful tools for constraint-based, nonempirical development of ground-state approximate functionals. In particular, the ground-state limit of the VT84F functional [28] was developed to meet those constraints (as well as others) for realistic atomic densities. Such densities have cusps at the nuclei [31]. VT84F therefore is nonuniversal in the particular sense in which "universal" is used in DFT. VT84F was adapted, by construction, to properties of the densities characteristic of bare Coulomb external potentials.

By design, the pseudodensities almost always used in AIMD calculations do not have such Coulombic cusps. Instead they have zero gradients at the origin. In that computational setting, VT84F (at $T=0$ K) can perform unreliably. Our response was to put forth the LKT ground-state functional [10]. It was formulated specifically to meet the rigorous positivity constraints in conjunction with ordinary pseudodensities.

In the present work we use the free energy GGA methodology [9] just summarized to promote LKT [10] into a free energy density functional "LKTF." The LKT enhancement factor is

$$F_\theta^{\rm LKT}(s)=1/\cosh(as)\quad\text{with}\ \ a=1.3. \tag{24}$$

Specifically, we have used the variables in Eqs. (16) and (17) and the approximate relationship Eq. (21) between F_τ and F_σ.

III. COMPUTATIONAL DETAILS

The calculations were of two types. One is electronic free energy minimization in the field of static ions ("static lattice"). The other is AIMD. All the calculations used the ground-state Perdew-Zunger local density approximation for the XC free energy functional [32] without explicit temperature dependence. This choice (the ground-state approximation) is for clarity of comparison among noninteracting functionals. In calculations for actual materials properties, proper free energy XC functionals should be used [24,33].

The static lattice OF calculations were done using a locally modified version of the PROFESS [34] code with finite-temperature capability. Comparison finite-T KS calculations were done with ABINIT version 8.8 [35]. We chose two representative simple elements, face-centered cubic (fcc) Al and cubic diamond (cd) Si. Both conventional KS and OF calculations used the BLPS [36] local pseudopotential. The KS calculations used plane wave energy cutoffs of 800 and 850 eV for Al and Si, respectively. Monkhorst-Pack k-point sampling convergence was used with four atoms in fcc symmetry with a $15\times15\times15$ grid and eight atoms in cd symmetry with a $9\times9\times9$ grid. Temperatures were from 1 to 10 eV in 1 eV increments. For Al, the bulk density range was 2.3 to 3.3 g/cm^3 sampled at 0.2 g/cm^3 intervals. The corresponding values for Si were 2.0 to 2.6 g/cm^3 at 0.1 g/cm^3 intervals. All bands with occupation $\geqslant 10^{-6}$ were included. The resulting number of bands used is listed in the Supplemental Material [29].

OF calculations were done with a representative group of one-point noninteracting free energy density functionals: TF, Perrot (i.e., TF$\frac{1}{9}$vW), TF$\frac{1}{5}$vW, VT84F, and LKTF. The TFλvW forms were implemented via the finite-T methodology summarized above and with Eq. (21), which is exact for those forms. In addition, we include a relatively recently developed nonlocal (two-point) noninteracting functional which has had some success [37]. We denote it as SDβ-vW14F.

The AIMD calculations were for the equation of state (EOS) of hydrogen (H), deuterium (D), and Al. Whether driven by conventional KS or OFDFT forces, the calculations were performed on the same footing with the PROFESS@QUANTUM-ESPRESSO package [38] and the same ground-state XC functional (PZ) as in the static cases. The bulk densities used were chosen such that the D EOS results could be compared with published PIMC values [39]. For H and D, in both the KS-AIMD and OF-AIMD calculations, the electron-ion interaction was treated via a deep local pseudopotential [38] with core radius 0.25 bohr. For Al, the KS-AIMD calculations used the nonlocal PAW dataset (Al.pz-n-kjpaw_psl.0.1.UPF) [40], and the PZ XC functional, while the OF-AIMD calculations used the aforementioned BLPS.

All the orbital-free calculations used a real-space grid size of 64^3 or 96^3 for H(D) and 128^3 for Al depending on the bulk densities. The number of atoms was 108 for H and D and 128 for Al. The time step varied from 0.0126 to 0.357 fs. Γ-point sampling was used for the KS-AIMD unless stated otherwise. Ion temperatures were regulated by Andersen thermostat. After equilibration, each system was run for 2000 steps. Pressures were averaged over those 2000 steps, yielding a maximum standard deviation relative to the average pressure of 5%.

IV. RESULTS

A. Computational cost

First, we consider the actual computational cost of OF-AIMD against KS-AIMD for H. For both types, the time per step was averaged over 6000 steps. The computations were performed on Intel E5-2698v3 processors with 4 GB of RAM per core. KS-AIMD used two nodes, while OF-AIMD used one. Each node comprised 32 cores. The wall time per step in units of minutes is shown in Fig. 1. The KS-AIMD cost actually grows exponentially, while the time per step of all the OF calculations (LKTF, VT84F, TF) is T independent. As expected, TF (not shown) runs fastest, a consequence of its simple locality. Typically LKTF requires fewer iterations to reach its converged electron density than the other semilocal functional, VT84F. That advantage is reflected in the wall time. A slight decrease in WALL time is observed for both LKTF and VT84F as T grows. We surmise that this is a consequence of growing homogeneity of the electron distribution as T increases but have not been investigated.

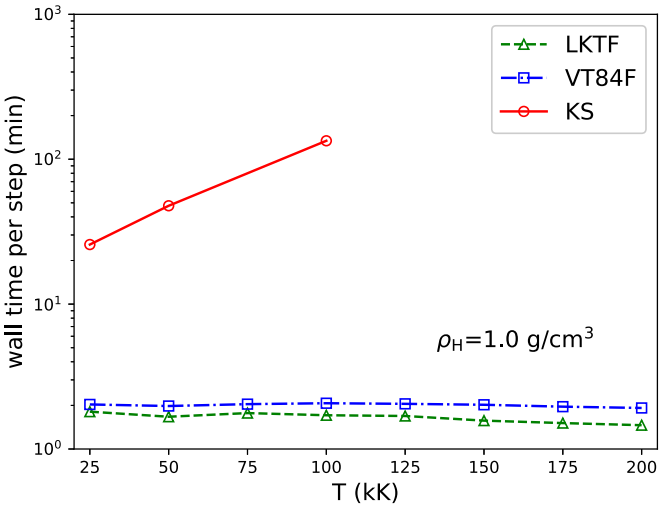

FIG. 1. Average WALL time per MD step as a function of T for ordinary KS-AIMD, and OF-AIMD with VT84F, and LKTF functionals. Hydrogen density is $\rho_H = 1.0$ g/cm^3. The KS cost grows while the LKTF and VT84F cost per step is T independent. As noted before, at $T = 0$ K, LKT SCF convergence is faster than VT84F.

B. Static lattice EOS

The main focus of this work is to make the free energy generalization of LKT and to explore its direct consequences. Improvements due to making alternative choices of ground-state kinetic energy density functionals, refined choice of XC functional, or alternative pseudopotential forms are outside the scope of the present report. Thus, for comparison we

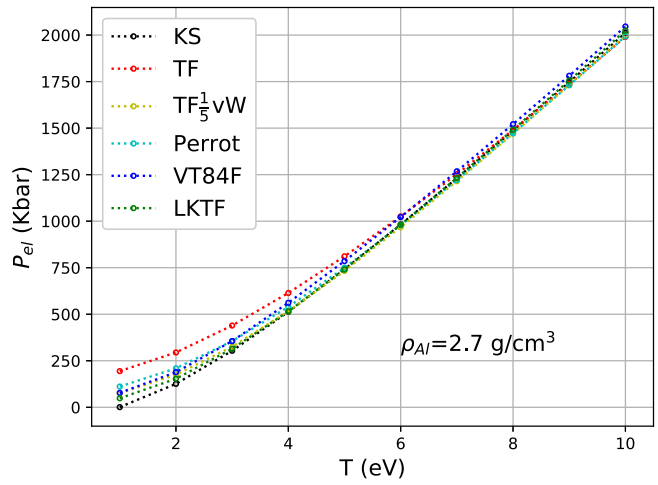

(a) isochoric

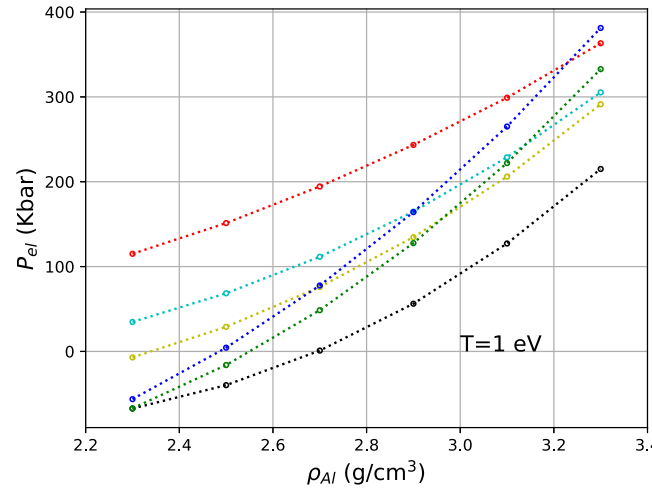

(b) isothermal

FIG. 2. Static lattice fcc Al electronic pressures from various OF functionals compared with conventional KS calculations. Top panel: Pressure as function of T for fixed material density $\rho = 2.7$ g/cm^3. Bottom panel: Isothermal pressure ($T = 1$ eV) as a function of material density.

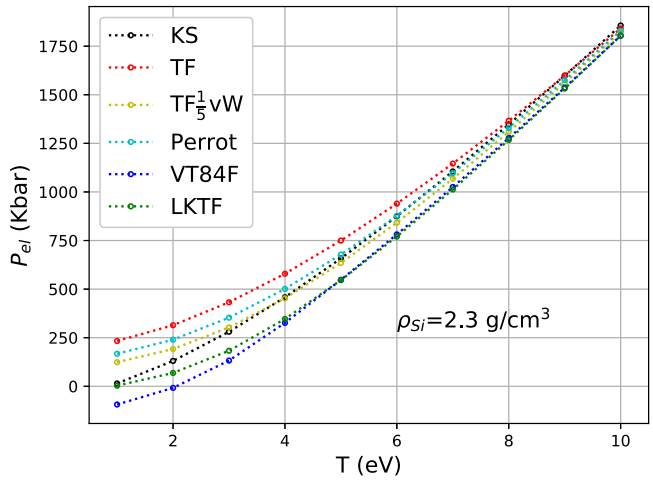

(a) isochoric

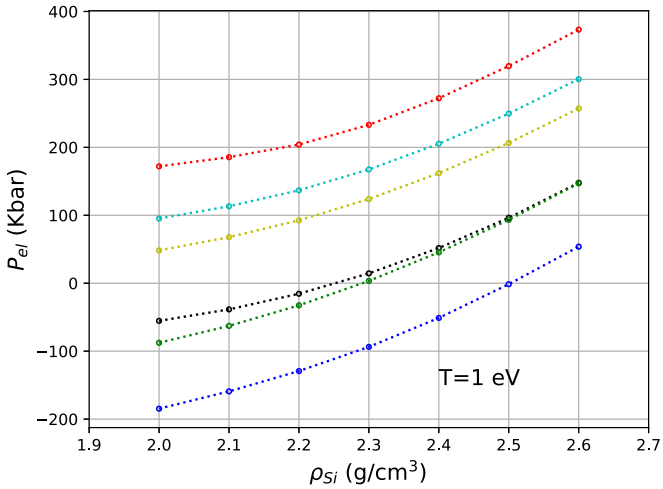

(b) isothermal

FIG. 3. Electronic pressure prediction comparison for various OF functionals compared with conventional KS results for static lattice cubic diamond (cd) Si. Top panel: Pressure as function of T for fixed material density $\rho = 2.3$ g/cm^3. Bottom panel: Isothermal pressure ($T = 1$ eV) as function of material density.

select a representative but clearly nonexhaustive set of kinetic energy density functionals.

1. fcc Al

As a representative case, for fcc Al we compared the electronic pressures of various OF functionals against those from the KS reference calculations. Figure 2(a) shows the results for bulk density $\rho = 2.7$ g/cm^3. Across the entire temperature range, of all the OF functionals LKTF stays closest to the KS data. At low temperatures, however, the OF functionals fail to reproduce the conventional KS results. To assess the performance of LKTF for slightly higher pressure and temperature, we analyzed the isothermal pressure at $T = 1$ eV for $2.3 \leqslant \rho \leqslant 3.3$ g/cm^3. See Fig. 2(b). From 2.2 to 2.9 g/cm^3, LKTF values remain closest to the conventional KS data, but for higher densities TF$\frac{1}{5}$vW is

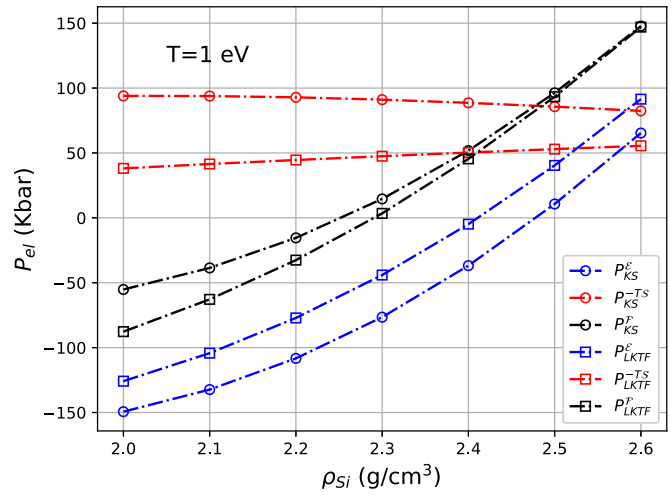

FIG. 4. Comparison of electronic pressure contributions from LKTF and conventional KS calculations for static cd Si at $T = 1$ eV. Superscript $\mathcal{E}$ denotes internal energy contribution, $T\mathcal{S}$ the entropic contribution, and $\mathcal{P}$ the total.

slightly better. Except for LKTF at the lowest density, none of the OF functionals does very well in this comparison.

All the data for this section, both for fixed ρ and fixed T, are included in the Supplemental Material.

2. cd Si

Figure 3(a) shows the electronic pressures for cd Si at $\rho = 2.3$ g/cm^3, close to the ambient bulk density. At $T = 1$ eV, among all the OF functionals, the LKTF pressure is almost identical to that from the conventional KS reference (Fig. 3(b)). However, as T grows, the LKTF EOS tends toward the VT84F EOS and the two are indistinguishable above $T \approx 4$ eV. Both lie below the conventional KS EOS. Whether this behavior is a shared flaw of the parent ground-state GGAs or is a sign of some limitation of the finite-T extension of the reduced gradient variable (summarized above) or some combination is unclear. In contrast, TFλvW approaches the KS EOS above $T \approx 3$ eV, with the choice of $\lambda = \frac{1}{5}$ outperforming $\lambda = \frac{1}{9}$ and $\lambda = 0$. Note however that TF$\frac{1}{5}$vW goes a bit below the conventional KS pressures above about $T = 5$ eV. Eventually, of course, everything goes to TF ($\lambda = 0$).

To gain understanding of these observations, we used the thermodynamic relation

$$P_{\rm el} = -\left.\frac{\partial \mathcal{F}_{\rm el}}{\partial V}\right|_{T,N} \tag{25}$$

to compute the pressure contributions from the internal energy $\mathcal{E}$ and entropic energy $-T\mathcal{S}$ and compare them to the counterpart quantifies from conventional KS calculations. Here $\mathcal{F}_{\rm el}$ is the electronic free energy, which conventionally is defined to be $\mathcal{F}_{\rm el} = \mathcal{F} + E_{\text{ion-ion}} + \int d\mathbf{r}\, v(\mathbf{r}) n(\mathbf{r})$ with $\mathcal{F}$ as defined in Eq. (2).

For $T = 1$ eV, LKTF performs best over $2.0 \leqslant \rho \leqslant 2.6$ g/cm^3. See Fig. 4. However, this is a result of error cancellation. The LKTF pressure contribution from E underestimates that from conventional KS, while the entropic contribution does the opposite. However, Fig. 5 shows that for $T = 5$ eV, the Perrot functional clearly works better.

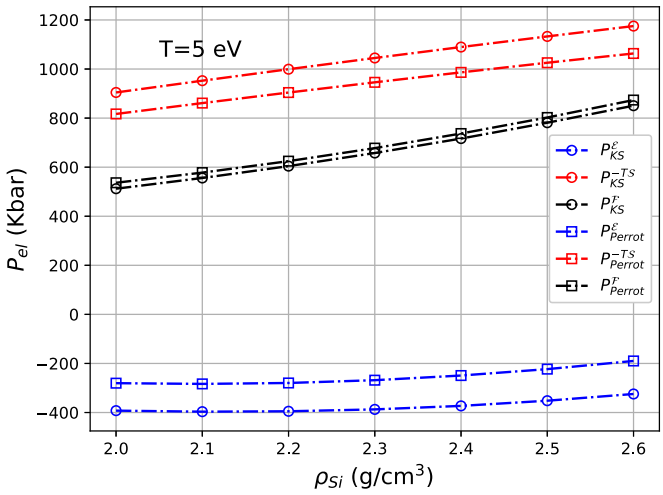

FIG. 5. As in Fig. 4 for the Perrot functional versus conventional KS calculations at $T = 5$ eV.

Even so, the thermodynamic contributions displayed in Fig. 5 show clearly that the comparatively good performance is a consequence of error cancellation between contributions both of which are rather far from the conventional KS values. Both cases shown also illustrate the underlying challenge: The conventional KS pressure is the result of significant cancellation of the two thermodynamic contributions.

C. *Ab initio* molecular dynamics

One of the strongest motivations for free energy OF-DFT is, as noted already, the prospect of linear scaling of AIMD calculation costs with respect to system size. Thus we turn from static lattice EOS to AIMD EOS calculations.

The EOS results for H from AIMD with the LKTF, VT84F, and conventional KS-AIMD treatments are plotted in Fig. 6 and tabulated in Table I. For $\rho = 0.6$ g/cm^3 and $T = 25$ kK, the relative error is reduced from 21% for VT84F to 11% for LKTF, roughly a factor of 2. As the temperature grows, the error from LKTF decreases from 11% to 6%, while as the density increases, the relative error rather quickly falls below 3.5%. This behavior is qualitatively similar to what was found for VT84F [28]. The pressure error relative to conventional KS-AIMD results decreases as the density and/or the temperature increases.

TABLE I. H pressure at various densities and two temperatures, $T = 25$ and 50 kK from AIMD simulations with LKTF, VT84F, and conventional KS. After equilibration, pressures were averaged over 2000 steps. An Andersen thermostat was used.

T (kK)	ρ_H (g/cm^3)	P_{KS}	P_{VT84F}	P_{LKTF} (Mbar)
25	0.6	2.1	1.7	1.9
	1.0	5.0	4.3	4.6
	2.0	16.9	15.7	16.3
	4.0	59.1	57.4	58.5
	8.0	207.2	204.1	205.8
50	0.6	3.9	3.5	3.6
	1.0	8.0	7.2	7.5
	2.0	22.7	21.5	22.2
	4.0	70.6	68.6	69.9
	8.0	229.5	226.5	228.3

For D, we chose two bulk densities $\rho_D = 1.96361$ ($r_s = 1.4$ bohrs), and $\rho_D = 4.04819$ g/cm^3 ($r_s = 1.1$ bohrs) for which PIMC data are available [39]. (Note that data from SDβ-vW14F calculations are unavailable for the lower density.) We remark that comparisons with the PIMC data involve the entire free energy functional utilized. Hence those comparisons may be distorted by our use of a simple ground-state LSDA XC functional. That possible problem does not arise in comparison with our KS-AIMD results, because those calculations used the same ground-state XC functional.

For the lower density, Fig. 7 displays the pressure as function of T relative to both KS-AIMD values (P/P_{KS}) and

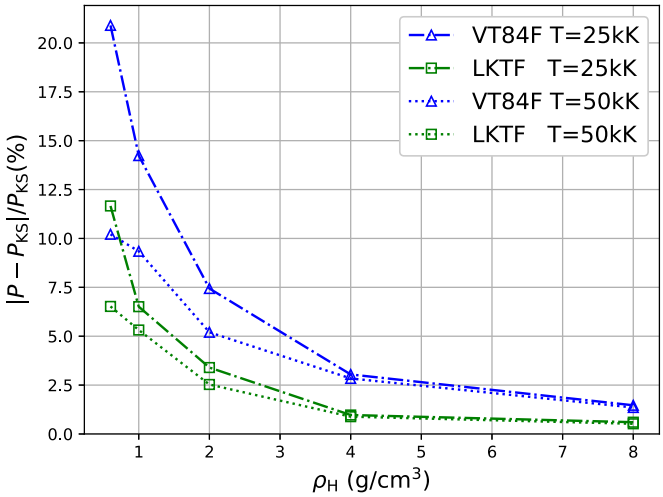

FIG. 6. Pressure error relative to KS-AIMD as function of bulk density for H with LKTF (squares) and VT84F (triangles) at $T = 25$ kK (dash-dotted curve) and 50 kK (dotted curve). Densities are 0.6, 1.0, 2.0, 4.0, and 8.0 g/cm^3,

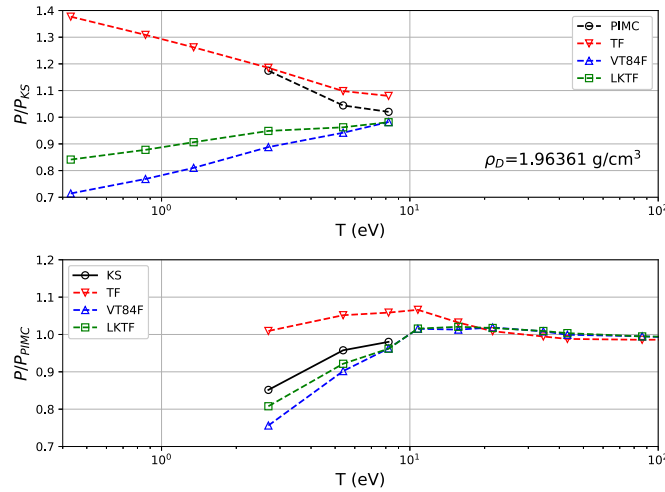

FIG. 7. Relative pressures versus temperature for D at $\rho = 1.96361$ ($r_s = 1.4$ bohrs) from PIMC, KS, LKTF, VT84F, and TF. Upper panel is relative to KS pressures, lower is relative to PIMC pressures.

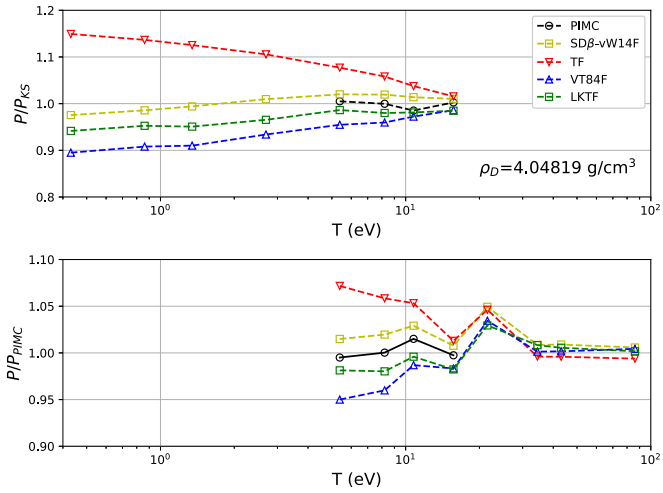

FIG. 8. As in Fig. 7 for D at $\rho = 4.04819$ g/cm^3 ($r_s = 1.1$ bohrs) and with SDβ-vW14F data as well.

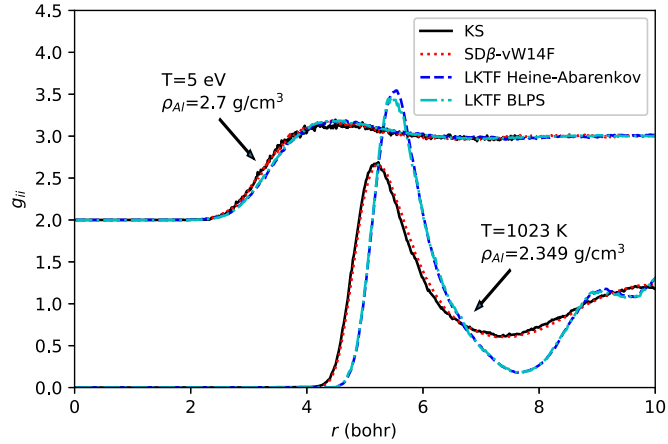

FIG. 9. Al radial distribution function (RDF) from LKTF (blue dash), KS (black solid), and SDβ-vW14F (red dotted) calculations for (a) $T = 5$ eV, $\rho = 2.7$ g/cm^3 and (b) $T = 1023$ K, $\rho = 2.349$ g/cm^3. The RDF for (b) is shifted upward by 2 for clarity of display.

relative to PIMC results ($P/P_{\rm PIMC}$). KS results are available up to $T = 95\,350$ K, ≈8.2 eV, while PIMC data are available only for $T \geqslant 31\,250$ K, ≈2.7 eV. At the lowest temperature, $T = 5$ kK (≈0.43 eV), LKTF underestimates the pressure by ≈15%, while VT84F is worse, at about 30%. TF, in contrast, drastically overestimates the low-T pressure by almost 40%. As T increases, the error from LKTF reduces quickly to an ≈5% underestimate at 31.25 kK with continuing reduction as T increases. The T dependence of $P/P_{\rm KS}$ for VT84F is similar, but with about twice the error of LKTF. As a caution, note in the upper panel of the figure that the PIMC pressure at $T =$ 31.25 kK deviates as much from the KS pressure as does the TF pressure. We believe that this deviation is a sign of well-known technical difficulties in PIMC for comparatively low temperatures. For $T \geqslant 100$ kK, however, PIMC indisputably is a reliable reference. In that regime both LKTF and VT84F are reasonably accurate. Both give pressures that approach TF values (by construction) for large T.

For the higher D density, Fig. 8 shows that the largest error relative to KS-AIMD pressure still is at the lowest temperature. LKTF underestimates the pressure by 7% at most, an error reduction of almost 2/3 compared to VT84F. As in the lower density case, TF again overestimates the low-T pressure, here by ≈14%. Relative to KS, the two-point functional SDβ-vW14F achieves better performance up to about $T = 50$ kK. Above that, LKTF is just as good. Relative to the PIMC results, LKTF performs as well or better than SDβ-vW14F.

For one further comparison, we also computed the radial distribution function (RDF) of Al for two sets of state conditions: (a) $T = 5$ eV, $\rho = 2.7$ g/cm^3, i.e, in the WDM regime; (b) $T = 1023$ K, $\rho = 2.349$ g/cm^3, i.e., near melting. Our calculations used the BLPS local pseudopotential, as before, as well as the Heine-Abarenkov [41,42] local pseudopotential. Figure 9 displays the results. In the lower-T case, LKTF overestimates the height of the first RDF peak relative to conventional KS value and shifts the peak position outward. This behavior is independent of detailed difference in the local pseudopotential. The BLPS and Heine-Abarenkov RDFs are virtually indistinguishable. Unsurprisingly, SDβ-vW14F does much better, an obvious consequence of its intrinsic nonlocality. For WDM conditions, LKTF delivers as good quality a RDF as the two-point functional SDβ-vW14F. Both are in good agreement with the conventional KS RDF. This again is plausible because of the great reduction in inhomogeneity upon going from $T \approx 0.09$ to 5 eV.

V. DISCUSSION AND SUMMARY

LKTF, the finite-T generalization of the LKT orbital-free kinetic energy density functional presented here, represents a significant advance over previously available one-point (semilocal) noninteracting free energy functionals. LKTF exploits nonuniversality in the form of specific adaptation to near-nucleus properties of pseudodensities. As a consequence, in both static lattice and AIMD calculations on a few elemental systems, LKTF substantially reduces errors versus KS or KS-AIMD compared to the previous best semilocal form, VT84F. Both of those constraint-based functionals deliver performance substantially superior to TF. At least for the Al RDF in the WDM regime, LKTF does as well as the nonlocal SDβ-vW14F. Wider usage of LKTF is needed both to exploit its advantages and identify limitations.

The improved performance of LKTF (relative to VT84F as the prior benchmark) is obtained at least in part by error cancellation between the kinetic and entropy contributions to the noninteracting free energy. Such cancellation may be system dependent, so reducing cancellation substantially while maintaining fidelity to conventional finite-T KS results is an important goal. Two other matters of investigation are suggested by the LKTF performance. One is whether the approximation of using Eq. (21) is inadequate and needs to be supplanted by solution of the exact thermodynamic relation between F_σ and F_τ. Second is whether the methodology of Ref. [9] has some unrecognized limitation that impacts the construction of functionals such as VT84F and LKTF.

ACKNOWLEDGMENTS

All the computations were performed on the University of Florida Research Computing HiPerGator-II system. We thank Travis Sjostrom for generously providing the SDβ-vW14F radial distribution function data. The majority of the work reported here was done while KL was at the University Florida. Both he and S.B.T. were supported by U.S. Department of Energy Grant DE-SC 0002139. V.V.K. acknowledges support by the Department of Energy National Nuclear Security Administration under Award No. DE-NA0003856.

[1] F. Graziani, M. P. Desjarlais, R. Redmer, and S. B. Trickey, *Frontiers and Challenges in Warm Dense Matter* (Springer Science & Business, New York, 2014), Vol. 96.

[2] R. Baer, D. Neuhauser, and E. Rabani, Self-Averaging Stochastic Kohn-Sham Density-Functional Theory, Phys. Rev. Lett. **111**, 106402 (2013).

[3] Y. Cytter, E. Rabani, D. Neuhauser, and R. Baer, Stochastic density functional theory at finite temperatures, Phys. Rev. B **97**, 115207 (2018).

[4] P. Hohenberg and W. Kohn, Inhomogeneous electron gas, Phys. Rev. **136**, B864 (1964).

[5] W. Kohn and L. J. Sham, Self-consistent equations including exchange and correlation effects, Phys. Rev. **140**, A1133 (1965).

[6] N. D. Mermin, Thermal properties of the inhomogeneous electron gas, Phys. Rev. **137**, A1441 (1965).

[7] A. Nakata, Y. Futamura, T. Sakurai, D. R. Bowler, and T. Miyazaki, Efficient calculation of electronic structure using o (n) density functional theory, J. Chem. Theory Comput. **13**, 4146 (2017).

[8] M. Levy and Hui Ou-Yang, Exact properties of the pauli potential for the square root of the electron density and the kinetic energy functional, Phys. Rev. A **38**, 625 (1988).

[9] V. V. Karasiev, T. Sjostrom, and S. B. Trickey, Generalized-gradient-approximation noninteracting free-energy functionals for orbital-free density functional calculations, Phys. Rev. B **86**, 115101 (2012).

[10] K. Luo, V. V. Karasiev, and S. B. Trickey, A simple generalized gradient approximation for the noninteracting kinetic energy density functional, Phys. Rev. B **98**, 041111(R) (2018).

[11] K. Luo and S. Trickey, Trivial constraints on orbital-free kinetic energy density functionals, Chem. Phys. Lett. **695**, 190 (2018).

[12] L. A. Constantin, E. Fabiano, and F. Della Sala, Semilocal Pauli-Gaussian kinetic functionals for orbital-free density functional theory calculations of solids, J. Phys. Chem. Lett. **9**, 4385 (2018).

[13] W. Mi, A. Genova, and M. Pavanello, Nonlocal kinetic energy functionals by functional integration, J. Chem. Phys. **148**, 184107 (2018).

[14] W. Mi and M. Pavanello, Orbital-free density functional theory correctly models quantum dots when asymptotics, nonlocality, and nonhomogeneity are accounted for, Phys. Rev. B **100**, 041105(R) (2019).

[15] J. Lehtomäki and O. Lopez-Acevedo, Semilocal kinetic energy functionals with parameters from neutral atoms, Phys. Rev. B **100**, 165111 (2019).

[16] W. C. Witt and E. A. Carter, Kinetic energy density of nearly free electrons. I. Response functionals of the external potential, Phys. Rev. B **100**, 125106 (2019).

[17] W. C. Witt and E. A. Carter, Kinetic energy density of nearly free electrons. II. Response functionals of the electron density, Phys. Rev. B **100**, 125107 (2019).

[18] W. C. Witt, K. Jiang, and E. A. Carter, Upper bound to the gradient-based kinetic energy density of noninteracting electrons in an external potential, J. Chem. Phys. **151**, 064113 (2019).

[19] L. A. Constantin, E. Fabiano, S. Śmiga, and F. Della Sala, Jellium-with-gap model applied to semilocal kinetic functionals, Phys. Rev. B **95**, 115153 (2017).

[20] L. A. Constantin, E. Fabiano, and F. Della Sala, Nonlocal kinetic energy functional from the jellium-with-gap model: Applications to orbital-free density functional theory, Phys. Rev. B **97**, 205137 (2018).

[21] V. V. Karasiev, T. Sjostrom, J. Dufty, and S. B. Trickey, Accurate Homogeneous Electron Gas Exchange-Correlation Free Energy for Local Spin-Density Calculations, Phys. Rev. Lett. **112**, 076403 (2014).

[22] S. Groth, T. Dornheim, T. Sjostrom, F. D. Malone, W. M. C. Foulkes, and M. Bonitz, *Ab Initio* Exchange-Correlation Free Energy of the Uniform Electron Gas at Warm Dense Matter Conditions, Phys. Rev. Lett. **119**, 135001 (2017).

[23] V. V. Karasiev, S. B. Trickey, and J. W. Dufty, Status of free-energy representations for the homogeneous electron gas, Phys. Rev. B **99**, 195134 (2019).

[24] V. V. Karasiev, J. W. Dufty, and S. B. Trickey, Nonempirical Semilocal Free-Energy Density Functional for Matter Under Extreme Conditions, Phys. Rev. Lett. **120**, 076401 (2018).

[25] R. P. Feynman, N. Metropolis, and E. Teller, Equations of state of elements based on the generalized Fermi-Thomas theory, Phys. Rev. **75**, 1561 (1949).

[26] J. Blakemore, Approximations for Fermi-Dirac integrals, especially the function F12 (η) used to describe electron density in a semiconductor, Solid-State Electron. **25**, 1067 (1982).

[27] J. Bartel, M. Brack, and M. Durand, Extended Thomas-Fermi theory at finite temperature, Nucl. Phys. A **445**, 263 (1985).

[28] V. V. Karasiev, D. Chakraborty, O. A. Shukruto, and S. B. Trickey, Nonempirical generalized gradient approximation free-energy functional for orbital-free simulations, Phys. Rev. B **88**, 161108(R) (2013).

[29] See Supplemental Material at http://link.aps.org/supplemental/10.1103/PhysRevB.101.075116 for a table left-hand vs right-hand side values for the approximate equation. Also provided are the number of bands used in the KS calculations.

[30] F. Perrot, Gradient correction to the statistical electronic free energy at nonzero temperatures: Application to equation-of-state calculations, Phys. Rev. A **20**, 586 (1979).

[31] T. Kato, On the eigenfunctions of many-particle systems in quantum mechanics, Commun. Pure Appl. Math. **10**, 151 (1957).

[32] J. P. Perdew and A. Zunger, Self-interaction correction to density-functional approximations for many-electron systems, Phys. Rev. B **23**, 5048 (1981).

[33] V. V. Karasiev, L. Calderín, and S. B. Trickey, Importance of finite-temperature exchange-correlation for warm dense matter calculations, Phys. Rev. E **93**, 063207 (2016).

[34] M. Chen, J. Xia, C. Huang, J. M. Dieterich, L. Hung, I. Shin, and E. A. Carter, Introducing profess 3.0: An advanced program for orbital-free density functional theory molecular dynamics simulations., Comput. Phys. Commun. **190**, 228 (2015).

[35] X. Gonze, F. Jollet, F. A. Araujo, D. Adams, B. Amadon, T. Applencourt, C. Audouze, J.-M. Beuken, J. Bieder, A. Bokhanchuk *et al.*, Recent developments in the abinit software package, Comput. Phys. Commun. **205**, 106 (2016).

[36] C. Huang and E. A. Carter, Transferable local pseudopotentials for magnesium, aluminum and silicon, Phys. Chem. Chem. Phys. **10**, 7109 (2008).

[37] T. Sjostrom and J. Daligault, Fast and Accurate Quantum Molecular Dynamics of Dense Plasmas Across Temperature Regimes, Phys. Rev. Lett. **113**, 155006 (2014).

[38] V. V. Karasiev, T. Sjostrom, and S. B. Trickey, Finite-temperature orbital-free DFT molecular dynamics: Coupling profess and quantum espresso, Comput. Phys. Commun. **185**, 3240 (2014).

[39] S. X. Hu, B. Militzer, V. N. Goncharov, and S. Skupsky, First-principles equation-of-state table of deuterium for inertial confinement fusion applications, Phys. Rev. B **84**, 224109 (2011).

[40] A. D. Corso, Pseudopotentials periodic table: From H to Pu, Comput. Mater. Sci. **95**, 337 (2014).

[41] V. Heine and I. V. Abarenkov, A new method for the electronic structure of metals, Philos. Mag.: J. Theor. Exp. Appl. Phys. **9**, 451 (1964).

[42] L. Goodwin, R. J. Needs, and V. Heine, A pseudopotential total energy study of impurity-promoted intergranular embrittlement, J. Phys.: Condens. Matter **2**, 351 (1990).